J Electroceram (2010) 24:76–82
DOI 10.1007/s10832-008-9455-9

Enhancement of thermoelectric performance in rare earth-doped $Sr_3Ti_2O_7$ by symmetry restoration of TiO_6 octahedra

Yifeng Wang · Kyu Hyoung Lee · Hideki Hyuga · Hideki Kita · Hiromichi Ohta · Kunihito Koumoto

Received: 26 October 2007 / Accepted: 13 February 2008 / Published online: 11 March 2008

Abstract Aiming at the realization of the enhancement of thermoelectric performance through structural modification, the present work has clarified the significant effects of rare earth (*RE*=Gd, Sm, Nd, and La) doping at Sr-sites in $Sr_3Ti_2O_7$, both on the structural restoration of distorted TiO_6 octahedra and on the Seebeck coefficient, especially at high temperatures. The preferential substitution of RE^{3+} at the nine-coordinate Sr-sites can facilitate the degeneration of the conduction band (Ti 3*d*-t_{2g}) orbital, owing to its special capability in restoring TiO_6 octahedra to a higher state of symmetry and thus enhance the density of states (DOS) effective mass of the carriers, which gives rise to a rather large increase in the Seebeck coefficient. The present findings have affirmed the effectiveness of structural restoration in enhancing the Seebeck coefficient by Sr-site-doping, which will help establish a useful solution for Ti-based thermoelectric oxides with inherently distorted TiO_6 octahedra to achieve high thermoelectric performance.

Keywords Ruddlesden-Popper phase · TiO_6 octahedra · Local symmetry · Thermoelectric properties

Y. Wang · H. Ohta · K. Koumoto
Graduate School of Engineering, Nagoya University,
Furo-cho, Chikusa,
Nagoya 464-8603, Japan

K. H. Lee · H. Ohta · K. Koumoto (✉)
CREST-Japan Science and Technology Agency,
4-1-8 Honcho,
Kawaguchi 332-0012, Japan
e-mail: koumoto@apchem.nagoya-u.ac.jp

H. Hyuga · H. Kita
National Institute of Advanced Industrial
Science and Technology (AIST),
2266 Anagahora, Shimo-Shidami Moriyama,
Nagoya 463-8560, Japan

1 Introduction

Thermoelectrics (TE) have been intensively investigated to achieve the goal of maximizing the dimensionless figure of merit, *ZT* ($ZT = S^2 \cdot \sigma \cdot T \cdot \kappa^{-1}$, where *Z*, *S*, σ, and κ are, respectively, a figure of merit, the Seebeck coefficient, the electrical conductivity, and the thermal conductivity at a given absolute temperature *T*; $ZT \geq 1$ is regarded as a criterion for practical application) so as to realize the high efficiency in power generation and solid-state refrigeration, and the essential technical difficulty is due to the trade-off dependences of *S*, σ and κ on the carrier concentration (n_e).

Although recognized as potential candidates for high temperature TE application due to their non-toxicity and high thermal stability, degenerate semiconducting metal oxides have experienced a long inactive period, owing to their low efficiency, until the unexpected discovery of high TE performance, comparable to metallic alloys, in the *p*-type Na_xCoO_2 [1], which has triggered an increasing interest in the field of TE oxides. In the *n*-type cubic perovskite-type $SrTi_{0.8}Nb_{0.2}O_3$ has been reported to exhibit a fairly high power factor ($S^2\sigma \sim 1.5\times10^{-3}$ W m^{-1} K^{-2} at 1000 K), benefiting from a large DOS effective mass ($m_d^* \sim 6-7\,m_o$, where m_o is the free electron mass) and its good structural tolerance toward heavy doping [2–4]. However, its maximum *ZT* value (~0.37 at 1000 K), although highest among the *n*-type TE oxides so far, is still insufficient for practical application. One way to further improve the *ZT* value is to enhance the power factor, very recently, a giant $|S|$ value ($|S|_{300\ K}$=850 μVK^{-1}, about five times larger than that of bulk $SrTiO_3$ at 300 K) has been realized, while maintaining a high σ_{2DEG}, to reach an amazingly large $ZT_{300\ K}$=~2.4 by using a high-density two-dimensional electron gas (2DEG) in Sr–Ti–O system [5]. Another effective way to a higher *ZT*, is to reduce the κ,

e.g., by employing a superlattice structure so as to enhance the phonon scattering effect at the numerous interfaces, while not deteriorating the S and σ. Therefore, Ruddlesden-Popper (RP) phases of Sr–Ti–O system were focused on.

The RP phases $SrO(SrTiO_3)_n$ or $Sr_{n+1}Ti_nO_{3n+1}$ (n = integer) are a family of layered perovskite-type natural superlattices that repeat alternatively a single NaCl-type SrO layer and n layers of perovskite-type $SrTiO_3$ along the c-axis [6, 7], with $SrTiO_3$ as the $n=\infty$ member, so that they should be capable not only of maintaining the excellent carrier transport features of $SrTiO_3$, but also of suppressing κ by effective phonon scattering at the $SrO/(SrTiO_3)_n$ interfaces [8].

Under these considerations, we previously studied the TE properties of Nb-doped (on Ti-sites) $SrO(SrTiO_3)_n$ (n= 1, 2) bulk ceramics [9, 10] and reported that the κ values were remarkably reduced in these compounds, by ~50% at RT and ~30% at 1000 K vs. the perovskite-type Nb-doped $SrTiO_3$, and the electrical conduction behavior was similar to that of $SrTiO_3$, but the $|S|$ and m_d^* values were fairly lower in these RP compounds, as were also observed in Nb-doped TiO_2 (anatase) [11]. This can be explained by the fact that the bottom of the conduction band (CB) for $SrTiO_3$ is composed of Ti $3d$-t_{2g} triply degenerate states [12]; however, the Ti $3d$-t_{2g} orbitals in these RP phases, e.g., the n=1 compound [13], split into two different states (i.e., the dispersion-less state, d_{xy}, and the other two energy-elevated dispersive states, d_{yz} and d_{zx}) due to crystal field splitting in the presence of distorted TiO_6 octahedra, which should be responsible for their small $|S|$ and m_d^*.

It can be deduced from the above that the presence of inherently irregular TiO_6 in the Ti-based TE oxides is the critical cause for their relatively low performance. On the other hand, these findings suggested a strategy to improve the TE performances for RP phases by restoring the local symmetry of the irregular TiO_6 octahedra; this was experimentally proven by the ZT improvement in Sr-site-Ca-substituted Nb-doped $Sr_3Ti_2O_7$ (i.e., the n=2 RP compound) [10].

In the present research, we prepared electron-doped $Sr_3Ti_2O_7$ dense bulk ceramics by non-isovalent substitution of rare earth ions (RE^{3+}) of various radii for Sr^{2+}, and explored the doping effect on improving the local symmetry of the TiO_6 octahedra over a wide temperature range, by the method of Rietveld refinement analysis. Furthermore, we studied the observed TE properties from the viewpoint of crystallographic characteristics, in an attempt to find a feasible way to improve the TE performance in $Sr_3Ti_2O_7$ and even for other TE oxides containing distorted TiO_6 octahedra.

2 Experimental

The stoichiometric starting powder mixtures of $SrCO_3$, TiO_2 and RE_2O_3 (RE=Gd, Sm, Nd and La) with a target composition of $(Sr_{0.95}RE_{0.05})_3Ti_2O_7$ were ball-mixed in ethanol solution for about 1 h. After being dried, the mixtures were preheated twice in air at 1200°C for 12 h with an intermediate grinding, and then were sintered two to three times at 1400–1450°C for 1–2 h in an Ar atmosphere, until a single phase composition was confirmed by XRD measurement; the resulting dark gray powders were finally hot-pressed at 1425°C under 35 MPa for 1 h in an Ar atmosphere into dense polycrystalline ceramic (5 mm in thickness and 45 mm in diameter, >96% of the theoretical density).

For the TE properties, the Seebeck coefficient (S) and electrical conductivity (σ) were simultaneously measured by a conventional steady-state method and a conventional dc four-probe method, respectively, with Au electrodes under an Ar atmosphere, in a temperature range of 300–1000 K, and the carrier concentration (n_e) and Hall mobility (μ_{Hall}) were determined with a van der Pauw configuration through Hall effect measurements under vacuum over the same temperature range.

To explain the RE^{3+} doping effect on the crystal structures, Rietveld analyses for all samples were conducted using the Rietan2000 program [14] for the detailed structural characteristics on room temperature X-ray diffraction (RT-XRD) data collected with a Rint2000 diffractometer (Rigaku Co., using Cu K_α) in the 10–100° 2θ range in steps of 0.02°. In addition, to compare the temperature dependences of the crystallographic parameters for RE-doped and Nb-doped $Sr_3Ti_2O_7$, in-situ high temperature X-ray diffraction (HT-XRD) measurements were conducted in the temperature range of 300–1000 K in steps of 100 K for $(Sr_{0.95}RE_{0.05})_3Ti_2O_7$ (RE=Sm and La) and $Sr_3(Ti_{0.9}Nb_{0.1})_2O_7$, on a 9 kW SmartLab (Rigaku Co., using Cu K_α) diffractometer with a DHS 900 domed hot stage heating attachment, and a Cu holder was employed to improve the thermal homogeneity. The samples were heated in a 100 ml/min N_2 flow at a 20 K/min rate to a desired temperature, after a 10 min hold for equilibration, the data were collected over the range of 2θ=10–120° at a 1.0°/min scan speed in steps of 0.02°. The HT-XRD data were then also analyzed by Rietveld refinement using the Rietan2000 program for lattice parameters and other crystallographic characteristics.

3 Results and discussion

3.1 Crystal structure characteristics

$Sr_3Ti_2O_7$ has a tetragonal crystal structure (space group, $I4/mmm$) alternating a NaCl-type SrO layer and a slab of perovskite-type $(SrTiO_3)_2$ along the c-axis. Figure 1 shows the schematic structure of (a) $Sr_3Ti_2O_7$, the TiO_6 octahedra

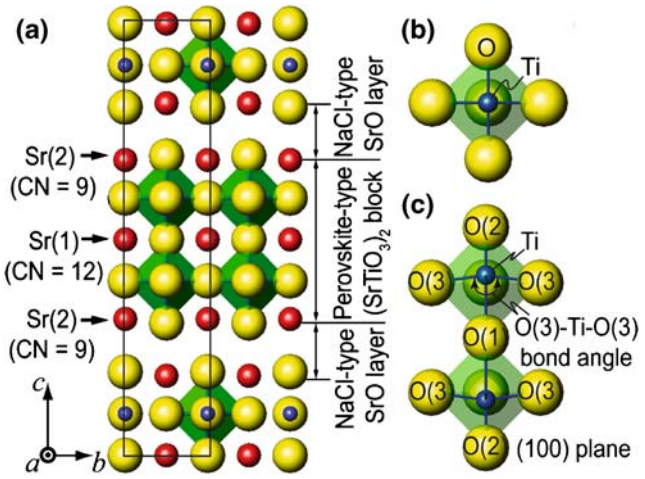

Fig. 1 Schematic illustrations for (**a**) crystal structure of $Sr_3Ti_2O_7$, (**b**) the regular TiO_6 octahedra in cubic perovskite-type $SrTiO_3$, and (**c**) the distorted TiO_6 octahedra in $Sr_3Ti_2O_7$. In $Sr_3Ti_2O_7$, there are two types of Sr-sites with coordination numbers of 12 and 9, located within the perovskite-type $(SrTiO_3)_2$ slab and along the interfaces between the $(SrTiO_3)_2$ slabs and the SrO layers, respectively

in (b) cubic perovskite-type $SrTiO_3$ and (c) the $(SrTiO_3)_2$ slab of $Sr_3Ti_2O_7$. The Sr atoms lie in either 12-coordinate sites within $(SrTiO_3)_2$ slab, or in 9-coordinate sites along the interface between the $(SrTiO_3)_2$ slabs and the SrO layers. In cubic perovskite-type $SrTiO_3$, the TiO_6 octahedron has an ideally regular symmetry; however, those in the $(SrTiO_3)_2$ slabs of $Sr_3Ti_2O_7$ are distorted by Ti atoms shifting slightly toward the SrO layers, leaving 3 Ti–O bonds (Ti–O(1), Ti–O(2) and Ti–O(3)) unequal in length and the O(3)–Ti–O(3) bond slightly bent.

For the $(Sr_{0.95}RE_{0.05})_3Ti_2O_7$ (*RE*=Gd, Sm, Nd and La) compounds, the crystallographic characteristics at room temperature were obtained from the Rietveld analysis on the RT-XRD patterns, which confirmed the single phase composition in all samples, and in particular, the O(3)-Ti-O(3) bond angles in the (100) plane in these compounds were calculated geometrically to evaluate the local symmetry of the TiO_6 octahedra by use of the results of the Rietveld analysis. Deviation from the perfect 180° angle observed in cubic perovskite $SrTiO_3$ is a sensitive measure of the symmetry of the TiO_6 octahedra. The reliability factors R_{wp} were ~10% in all compounds. The crystallographic results obtained are illustrated in Fig. 2.

The lattice parameters (*a* and *c*) and the lattice volume (*V*) expand gradually with the increase in the RE^{3+} radii ($r_{Gd^{3+}} = 1.107$ Å, $r_{Sm^{3+}} = 1.131$ Å, $r_{Nd^{3+}} = 1.163$ Å, $r_{La^{3+}} = 1.216$ Å; coordination number (CN)=9) [15]. Moreover, The O(3)-Ti-O(3) bond angles increase with decreasing RE^{3+} radius, which means that a higher symmetry of TiO_6 can be achieved by the substitution for Sr^{2+} with smaller RE^{3+} ions. It should be noted that the occupancy of doped RE^{3+} ions at 9-coordinate Sr-sites is found to be

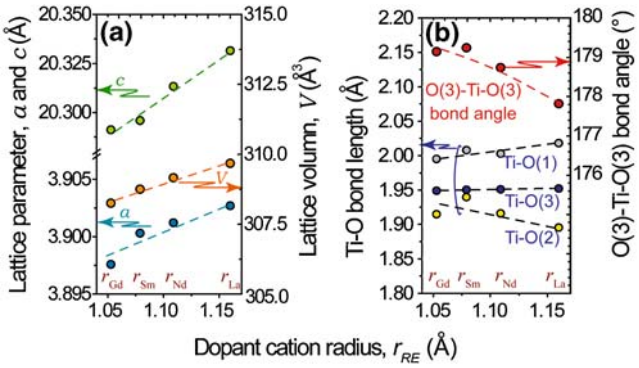

Fig. 2 Dependences of (**a**) lattice parameters (*a*, *c*, and *V*), and (**b**) Ti-O bond lengths and O(3)-Ti-O(3) bond angle on dopant ion radii (RE^{3+})

overwhelmingly larger than at 12-coordinate ones, and similar selective occupation of metal ions with smaller radii in the RP phases has frequently been reported [16]. This preferential positioning of RE^{3+} ions might be due to that their ion radii are close to that of 9-coordinate Sr^{2+} ($r_{Sr^{2+}} = 1.36$ Å; CN=9) as compared to that of 12-coordinate one ($r_{Sr^{2+}} = 1.44$ Å; CN=12).

To clarify the structural change of $(Sr_{0.95}RE_{0.05})_3Ti_2O_7$ at high temperature, the relevant crystallographic characteristics for $(Sr_{0.95}RE_{0.05})_3Ti_2O_7$ (*RE*=Sm and La) were derived from Rietveld analysis of the powder HT-XRD measurements and were compared with those for $Sr_3(Ti_{0.9}Nb_{0.1})_2O_7$, the Rietveld plots of $(Sr_{0.9}Sm_{0.05})_3Ti_2O_7$ at 300 K and 800 K are shown in Fig. 3.

Figure 4(a) shows the temperature dependence of *a*, *c* and *V*. The latter grows gradually with increasing temperature, as a result of the expansion in *a* and *c*, both in La- and Sm-doped $Sr_3Ti_2O_7$. It has been reported that no

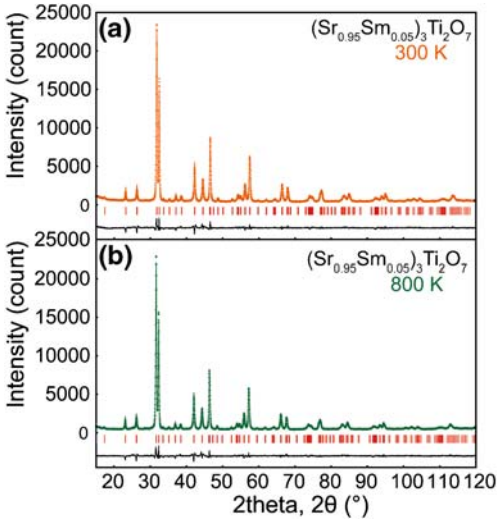

Fig. 3 Rietveld analysis plots for $(Sr_{0.95}Sm_{0.05})_3Ti_2O_7$ at (**a**) 300 K (R_{wp}=7.48%) and (**b**) 800 K (R_{wp}=7.16%). *Dots* represent the observed data points, and the *solid line* a calculated fit to the experiment data; the *bottom line* is the difference curve between observed and calculated values

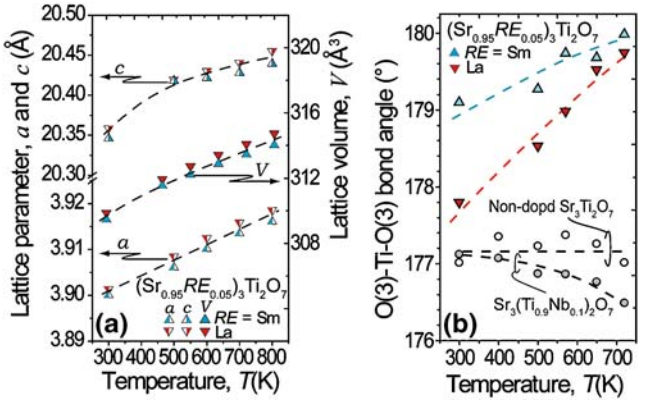

Fig. 4 Temperature dependences of (**a**) lattice parameters (*a, c* and *V*), and (**b**) O(3)-Ti-O(3) bond angle for $(Sr_{0.95}RE_{0.05})_3Ti_2O_7$ (*RE*=Sm, La)

perceivable change in the O(3)–Ti–O(3) bond angle in the (100) plane appeared in the non-doped $Sr_3Ti_2O_7$ when heated to a high temperature [10]. In contrast, the O(3)–Ti–O(3) bond angles in the (100) plane for the doped $Sr_3Ti_2O_7$ samples change diversely: (1) In the La-doped sample, it trends to increase gradually with increasing temperature, reaching an elevated value close to 180° at 1000 K, furthermore, the bond angle for the Sm-doped compound grows from an elevated starting point to an even larger end-angle at 1000 K; (2) Meanwhile, the bond angle in Nb-doped compound decreases reversely with temperature. These results imply that a higher symmetry of the TiO_6 octahedra can be achieved by doping $Sr_3Ti_2O_7$ at Sr-site with smaller RE^{3+} rather than at Ti-site with Nb^{5+}, especially at high temperatures.

3.2 Thermoelectric properties

Figure 5(a) shows the temperature dependence of σ for $(Sr_{0.95}RE_{0.05})_3Ti_2O_7$ compounds, with the cubic perovskite-type La-doped $SrTiO_3$ [5] and $Sr_3(Ti_{0.9}Nb_{0.1})_2O_7$ [9] compounds as references, and the inset shows the temperature dependences of n_e and μ_{Hall}. In all of the $(Sr_{0.95}RE_{0.05})_3Ti_2O_7$ samples, σ decreases gradually with increasing temperature, suggesting that they are degenerate semiconductors. The σ values for the $(Sr_{0.95}RE_{0.05})_3Ti_2O_7$ compounds are rather lower than those of the Nb-doped $SrTiO_3$, which should be a result of the presence of insulating SrO layers distributed randomly in the polycrystalline $Sr_3Ti_2O_7$ ceramics. In the whole temperature range, the n_e values are generally constant at a same level ($n_e \sim 8\times10^{20}$ cm^{-3}). Above 700 K, the μ_{Hall} values decreases proportionally to $T^{-1.5}$ as a result of dominant acoustic electron-phonon scattering, similar to that in the cubic perovskite-type Nb-doped $SrTiO_3$, implying that the electron transport is occurring predominantly in the perovskite layers. Overall, the electrical conduction behavior for $(Sr_{0.95}RE_{0.05})_3Ti_2O_7$ is very similar to that in Nb-doped $Sr_3Ti_2O_7$ and $SrTiO_3$.

Figure 5(b) shows the temperature dependence of $|S|$ for the $(Sr_{0.95}RE_{0.05})_3Ti_2O_7$ samples, and that for the $Sr_3(Ti_{0.9}Nb_{0.1})_2O_7$ polycrystalline ceramic [9] is shown for comparison. All samples have negative S, with a gradual increase in magnitude with temperature, indicating that they are *n*-type degenerate semiconductors. Moreover, the S values for the $(Sr_{0.95}RE_{0.05})_3Ti_2O_7$ samples show behavior as follows: (1) at a given temperature, the $|S|$ values for the smaller *RE*(Gd and Sm)-doped samples are larger than those of the larger *RE*(Nd and La)-doped ones; (2) in the $(Sr_{0.95}RE_{0.05})_3Ti_2O_7$ samples, the $|S|$ values exhibit a larger increase rate with temperature than that in the Nb-doped $Sr_3Ti_2O_7$ compounds, especially in the high temperature region (above ~650 K).

In order to clarify these characteristics for the S values, the value of m^*_d, which is one of the main factors determining S, was estimated by the use of the following equations [17, 18]:

$$m^* = \frac{h^2}{2k_B T}\left[\frac{n_e}{4\pi F_{1/2}(\xi)}\right]^{2/3} \quad (1)$$

where h, k_B, F_n and ξ are the Plank constant, the Boltzmann constant, the Fermi integral, and the chemical potential, respectively. $F_n(\xi)$ and S can be expressed as

$$F_n(\xi) = \int_0^\infty \frac{x^n}{1+e^{x-\xi}}dx \quad (2)$$

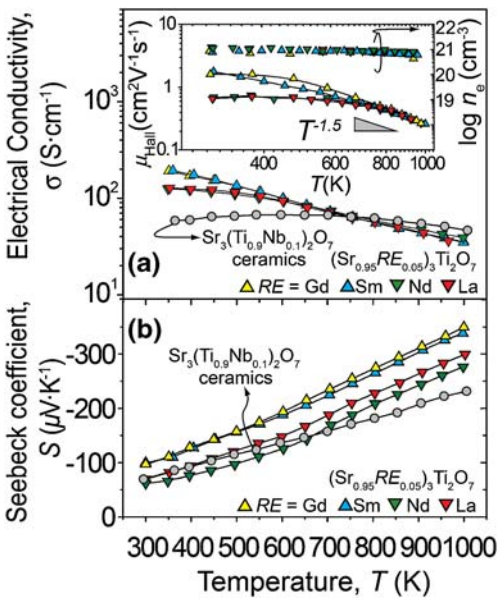

Fig. 5 Temperature dependences of (**a**) electrical conductivity (σ), and (**b**) Seebeck coefficient (S) for $(Sr_{0.95}RE_{0.05})_3Ti_2O_7$ (*RE*=Gd, Sm, Nd and La). The *insert* in (**a**) illustrates the variation of carrier concentration (n_e) and Hall mobility (μ_{Hall}) with temperature. The *circles* represents the data for $Sr_3(Ti_{0.9}Nb_{0.1})_2O_7$ ceramics from [9]

$$S = -\frac{k_B}{e}\left[\frac{(r+2)F_{r+1}(\xi)}{(r+1)F_r(\xi)} - \xi\right] \quad (3)$$

where e is the electron charge, and r is the carrier scattering parameter of relaxation time, which was assumed to be r=0 above 750 K, since the carriers are scattered only by acoustic phonons and r=0.5 at room temperature [19], while the intervening values (300–750 K) were estimated by interpolation based on a presumed linear dependence of r on temperature.

The temperature dependence of the m_d^* values for the $(Sr_{0.95}RE_{0.05})_3Ti_2O_7$ compounds were examined and are shown in Fig. 6(a). Overall, the smaller radius of RE doped, the relatively larger value of m_d^* is found in the compounds. Moreover, at room temperature, the m_d^* values are just slightly larger than those for 5% and 10% Nb-doped $Sr_3Ti_2O_7$ [9]. However, as temperature increases, the m_d^* values grow rapidly in the high temperature region (above 650 K) and reach a high value (~7.5 m_o at 900 K) near to that reported for the cubic perovskite-type $SrTiO_3$.

As shown in Fig. 7, the m_d^* value for cubic perovskite-type $SrTiO_3$ was reported to increase linearly with the Ti–Ti distance in [110], originating from carrier localization as a result of lattice expansion [4]; On the other hand, the m_d^* values in the Ti-site-Nb-doped $Sr_3Ti_2O_7$ are almost independent of the Ti-Ti distance [9]. While in Sr-site-*RE*-doped $Sr_3Ti_2O_7$ (e.g., *RE*=Sm, La), the m_d^* values are actually close to those of the Nb-doped RP phases, but as the Ti-Ti distances expand with increasing temperature, and the m_d^* values grow drastically to reach a high level comparable to the value for cubic perovskite-type $SrTiO_3$ at the same Ti–Ti distance.

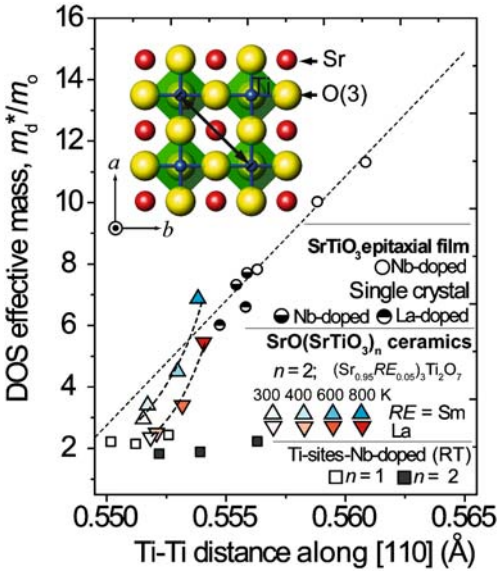

Fig. 7 Carrier DOS effective mass (m_d^*) data for $(Sr_{0.95}RE_{0.05})_3Ti_2O_7$ (*RE*=Sm and La) as a function of Ti–Ti distance along [110]. Data for $SrTiO_3$ and Ti-site-Nb-doped RP phases are cited from [5] and [9], respectively

We proposed in our previous work [9] that the small m_d^* values (~2.5 m_o) for the Nb-doped RP phases were caused by the crystal field splitting of the Ti 3*d*-t_{2g} orbitals (splitting of the degeneracy) in the distorted TiO_6 octahedra, and the effect of m_d^* increase with lattice expansion, originating from carrier localization, must be limited to the structures with high symmetry TiO_6 octahedra.

So the relationship between the m_d^* and the O(3)–Ti–O(3) bond angle was studied and is illustrated in Fig. 6(b). The value of m_d^* is nearly constant at low angles (< ~179°), while it increases sharply in the high angle region (179–180°), which corresponds to the highly symmetric state of the TiO_6 octahedra. This effect should be considered to be caused by the further degeneration induced in the Ti-3*d* orbitals as a result of the structurally restored TiO_6 octahedra.

It is reasonable to deduce thereby that the increase of m_d^* in $(Sr_{0.95}RE_{0.05})_3Ti_2O_7$ derives from structural modifications in two aspects to enhance the DOS at the CB bottom: primarily, the increase in the O(3)–Ti–O(3) bond angle, leading to a highly symmetrical state of the TiO_6 octahedra, which would facilitate the further degeneracy in the Ti-3*d*

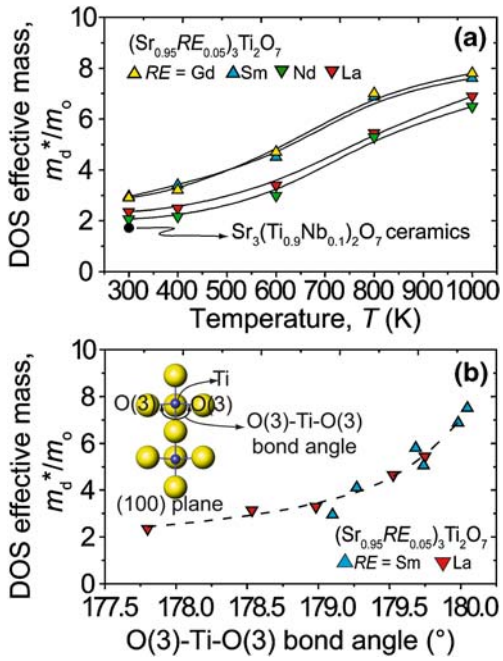

Fig. 6 Carrier DOS effective mass (m_d^*) variation with (**a**) temperature in $(Sr_{0.95}RE_{0.05})_3Ti_2O_7$ (*RE*=Gd, Sm, Nd and La), and (**b**) O(3)–Ti–O(3) bond angles in $(Sr_{0.95}RE_{0.05})_3Ti_2O_7$ (*RE*=Sm and La). The *circle* in (**a**) designates the data for $Sr_3(Ti_{0.9}Nb_{0.1})_2O_7$ ceramics quoted from [9]

orbitals, and secondarily, the accompanying expansion in the Ti–Ti distance at higher temperatures, which plays an effective role only in enhancing m_d^*, just under the prerequisite of the restored symmetry of the TiO_6 octahedra.

Figure 8(a) shows the temperature dependence of the $S^2\sigma$ for the $(Sr_{0.95}RE_{0.05})_3Ti_2O_7$ samples, with $Sr_3(Ti_{0.95}Nb_{0.05})_2O_7$ as reference [9]. Favored by the enhancement in S, the maximum $S^2\sigma$ (~430 μW K^{-2} m^{-1}) for $(Sr_{0.95}RE_{0.05})_3Ti_2O_7$, which was observed in $(Sr_{0.95}Gd_{0.05})_3Ti_2O_7$ at 1000 K, is ~40% larger than the maximum value obtained in $Sr_3(Ti_{0.95}Nb_{0.05})_2O_7$ at ~950 K (~300 μW K^{-2} m^{-1}) for the Ti-site-Nb-doped $SrO(SrTiO_3)_n$ (n=1, 2) [9].

Figure 8(b) presents the κ values for $(Sr_{0.95}Sm_{0.05})_3Ti_2O_7$, with data for $Sr(Ti_{0.8}Nb_{0.2})O_3$ and $Sr_3(Ti_{0.9}Nb_{0.1})_2O_7$ quoted for comparison. Overall, the κ for all $(Sr_{0.95}RE_{.05})_3Ti_2O_7$ (RE=Gd, Sm, Nd and La) are close to those for $Sr_3(Ti_{0.9}Nb_{0.1})_2O_7$ and are remarkably reduced by ~60% at room temperature and ~30% at 1000 K, as compared to those for $Sr(Ti_{0.8}Nb_{0.2})O_3$. Since the κ_{ele} values, the carriers contribution in κ, estimated by the Wiedemann–Franz law are very small (κ_{ele}~0.2 Wm^{-1}K^{-1}) compared with the total κ, κ_{tot}, which indicates that the phonon contribution is predominant, the reduction in κ for the RP compounds is believe to be caused by the enhanced phonon scattering effect at the internal interfaces of $SrO/(SrTiO_3)_2$.

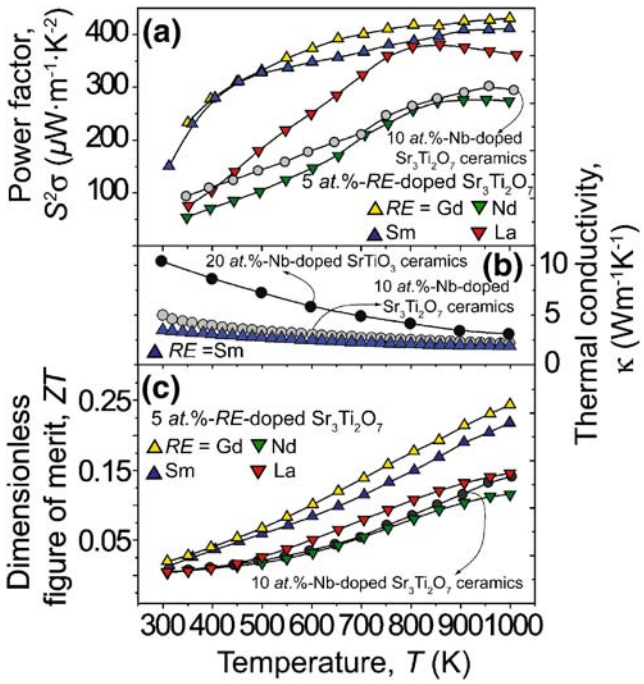

Fig. 8 Temperature dependences of (**a**) power factor ($S^2\sigma$), (**b**) thermal conductivity (κ), and (c) dimensionless figure of merit (ZT) for $(Sr_{0.95}RE_{0.05})_3Ti_2O_7$ (RE=Gd, Sm, Nd and La). Data for $Sr_3(Ti_{0.9}Nb_{0.1})_2O_7$ ceramics are quoted from [9], and the *black dots* in (**b**) represent the data for $Sr(Ti_{0.8}Nb_{0.3})O_3$ polycrystalline ceramics from [4]

From the observed S, σ, and κ, the ZT values were calculated and illustrated in Fig. 8(c). Benefiting from the greatly increased $S^2\sigma$, the ZT values for the Gd- and Sm-doped $Sr_3Ti_2O_7$ are rather larger than those both for Nd- and/or La-doped compounds and for $Sr_3(Ti_{0.9}Nb_{0.1})_2O_7$. Accordingly, the maximum ZT~0.24 obtained for $(Sr_{0.95}Gd_{0.05})_3Ti_2O_7$ at 1000 K is nearly 70% larger than the highest value reported for Ti-site-Nb-doped RP phases ($ZT_{1000\ K}$=0.14), and is even comparable to that of 5% Nb-doped $SrTiO_3$. Thus, in addition to its similar effects on the carrier transport properties and thermal properties as Ti-site Nb-doping, RE-doping on Sr-site in $Sr_3Ti_2O_7$ could effectively improve the local symmetry of TiO_6 octahedra, especially at high temperatures, so that it can further the degeneration of Ti 3d-t_{2g} orbitals to enhance m_d^* and $|S|$, leading to a fairly increased ZT value. Because the present σ values are rather smaller than those of $SrTi_{0.8}Nb_{0.2}O_3$ due to the presence of randomly distributed insulating SrO layers, the further effort will be taken for the processes for highly axis-orientated textured ceramics, single crystals or epitaxial thin films to achieve a high TE performance and clarify the intrinsic TE properties of RP phases.

4 Summary

$(Sr_{0.95}RE_{0.05})_3Ti_2O_7$ (RE=Gd, Sm, Nd, and La) dense ceramics were prepared with single phase, and their structural characteristics and thermoelectric parameters were investigated to clarify the RE^{3+} doping effect, both on the structural restoration of the TiO_6 octahedra and on the thermoelectric properties. The results revealed that the doping of RE^{3+} at the Sr-sites for $Sr_3Ti_2O_7$ was effective in improving the local symmetry of the TiO_6 octahedra, especially at high temperatures. The m_d^* values in these compounds were greatly enhanced, this could be considered to be due primarily to the improvement of the local symmetry of the TiO_6 octahedra and secondarily to the accompanying lattice thermal expansion, which furthered the degeneration of the Ti-3d orbitals. As a result, the $|S|$ values were remarkably enhanced, and the maximum ZT (~0.24 at 1000 K) obtained in $(Sr_{0.95}Gd_{0.05})_3Ti_2O_7$ was significantly larger than that for $Sr_3(Ti_{0.95}Nb_{0.05})_2O_7$ (~0.14 at 1000 K). These results are considered to be favorable in finding a solution to achieve high thermoelectric performance for $Sr_3Ti_2O_7$ and even for other Ti-based thermoelectric oxides containing irregular TiO_6 octahedra.

Acknowledgment The authors thank Dr. Katsuhiko Inaba (Rigaku Corporation) sincerely for his great effort in conducting the HT-XRD measurements and his instructive discussion of the data, and also thank Dr. Kouta Iwasaki (Nagoya University) wholeheartedly for his instruction on Rietveld refinement analysis.

References

1. I. Terasaki, Y. Sasago, K. Uchinokura, Phys. Rev. B. **56**(20), 685 (1997)
2. S. Ohta, T. Nomura, H. Ohta, M. Hirano, H. Hosono, K. Koumoto, Appl. Phys. Lett. **87**, 092108 (2005)
3. S. Ohta, H. Ohta, K. Koumoto, J. Ceram. Soc. Jpn. **114**, 102 (2006)
4. S. Ohta, T. Nomura, H. Ohta, K. Koumoto, J. Appl. Phys. **97**, 034106 (2005)
5. H. Ohta, S.W. Kim, Y. Mune, T. Mizoguchi, K. Nomura, S. Ohta, T. Nomura, Y. Nakanishi, Y. Ikuhara, M. Hirano, H. Hosono, K. Koumoto, Nat. Mater. **6**, 129 (2007)
6. S.N. Ruddlesden, P. Popper, Acta Crystallogr. **10**, 538 (1957)
7. S.N. Ruddlesden, P. Popper, Acta Crystallogr. **11**, 54 (1958)
8. K. Koumoto, S. Ohta, H. Ohta, *Proceedings of the 23rd International Conference on Thermoelectrics* (IEEE, Piscataway, 2005), p. 92
9. K.H. Lee, S.W. Kim, H. Ohta, K. Koumoto, J. Appl. Phys. **100**, 063717 (2006)
10. K.H. Lee, S.W. Kim, H. Ohta, K. Koumoto, J. Appl. Phys. **101**, 083707 (2007)
11. D. Kurita, S. Ohta, K. Sugiura, H. Ohta, K. Koumoto, J. Appl. Phys. **100**, 096105 (2006)
12. R. Asahi, Y. Taga, W. Mannstadt, A.J. Freeman, Phys. Rev. B **61**, 7459 (2000)
13. T. Schimizu, T. Yamaguchi, Appl. Phys. Lett. **85**, 1167 (2004)
14. F. Izumi, T. Ikeda, Mat. Sci. Forum **321**, 198 (2000)
15. R.D. Shannon, Acta Cryst. **A32**, 751 (1976)
16. K . Hawkins, T.J. White, Phys. Sci. Eng. **336**, 541 (1991)
17. V.I. Fistul, *Heavily Doped Semiconductors* (Plenum, New York, 1969)
18. C.B. Vining, J. Appl. Phys. **69**, 331 (1991)
19. K. Durczewski, M. Ausloos, Phys. Rev. B **61**, 5303 (2000)